Late Pliocene—Quaternary (<2.7 Ma) Sedimentation in the Eurasian Basin (Arctic Ocean)

A. V. Zayonchek^{a, b, *}, S. Yu. Sokolov^{a, **}, and A. V. Soloviev^{a, b}

^a Geological Institute, Russian Academy of Sciences, Moscow, 119017 Russia
^b All-Russia Research Geological Oil Institute, Moscow, 105118 Russia
*e-mail: a_zayonchek@mail.ru
**e-mail: sysokolov@yandex.ru

Received November 28, 2024; revised February 9, 2025; accepted February 19, 2025

Abstract—Geomorphological analysis and age correlation of the Late Pliocene—Quaternary regional stages identified in the ARC1407A seismic section by onlapping the oceanic basement, with the age specified based on calculations of the position of theoretical linear magnetic anomalies, were carried out. Interpretation of the ARC1407A seismic time section makes it possible to use the previous seismostratigraphic correlations of glaciomarine deposits for the western Barents Sea and the northeastern part of the adjacent deep-water basin. Based on the geomorphological analysis, extended canyon systems were identified in the Nansen Basin and eastern Amundsen Basin. Significant amounts of sedimentary cover in the Nansen Basin are glaciomarine sediments deposited since the end-Late Pliocene. In the central Nansen Basin, glaciomarine sediments, transported to the central Nansen Basin cyclically, have a mixed character (underwater landslides and turbidite flows). In the Amundsen and Podvodnikov basins, glaciomarine deposits began to form in the second half of the Middle Neopleistocene.

Keywords: Arctic Ocean, Eurasian Basin, Gakkel Ridge, Amundsen Basin, Nansen Basin, spreading, theoretical axes of linear magnetic anomalies, sedimentary cover, seismic stratigraphy, Late Pliocene—Quaternary

DOI: 10.1134/S002449022570021X

INTRODUCTION

The North Arctic Ocean (NAO) includes two deep-sea (Amerasian and Eurasian) basins separated by the Lomonosov Ridge. According to the majority of geologists and geophysicists, the Eurasian Basin was formed in the Cenozoic due to the spreading of the North American (Lomonosov Ridge included) and Eurasian plates (Gaina, 2002; Glebovsky, 2006; Karasik, 1974; Merkouriev and DeMets, 2014; Nikishin, 2018; Zayonchek et al., 2023).

The Eurasian Basin is characterized by the presence of a thick sedimentary cover not only in deep-sea basins (Castro, 2018; Engen, 2009; Funck, 2022), but also within the central and eastern parts of the Gakkel Ridge rift valley up to its junction with the Laptev Sea rift system (Jokat and Micksch, 2004; Nikishin, 2018; Rekant and Gusev, 2016; Sekretov, 2002).

A significant part (30–60% of the total thickness) of the sedimentary cover in the western and central parts of the Nansen Basin adjacent to the northern margin of the Barents Sea, as well as in the eastern part of the basin in the northern Norway—Greenland Basin adjacent to the western margin of the Barents Sea (Fig. 1),

is composed of Late Pliocene—Quaternary (<2.7 Ma) glaciomarine deposits (Alexandropoulou et al., 2021; Amundsen et al., 2011; Engen, 2009; Faleide et al., 1996; Fiedler and Faleide, 1996; Lasabuda et al., 2021; Zayonchek and Merkouriev, 2021; Zayonchek et al., 2023). These rocks were recovered by boreholes (Fig. 1) drilled on the western continental margin of the Barents Sea, within the northern Norway-Greenland Basin and on the Yermak Plateau, which made it possible to accomplish their stratigraphic and seismostratigraphic correlations (Alexandropoulou et al., 2021; Butt et al., 2000; Channell et al., 1999; Eidvin and Nagy, 1999; Faleide et al., 1996; Forsberg et al., 1999; Geissler and Jokat, 2004; Jansen et al., 1996; Knies et al., 2009; Mattingsdal et al., 2014; Medvedev et al., 2023; Myhre et al., 1995; Rebesco et al., 2014).

When interpreting seismic data on the western part of the Nansen Basin in the Eurasian glaciomarine basin, Late Pliocene—Quaternary deposits were distinguished based on their correlation with sections of boreholes drilled on the Yermak Plateau, where two seismic complexes, separated by a boundary with an age of ~1.5 Ma, were identified (Engen, 2009). The purpose of present study is to accomplish a more

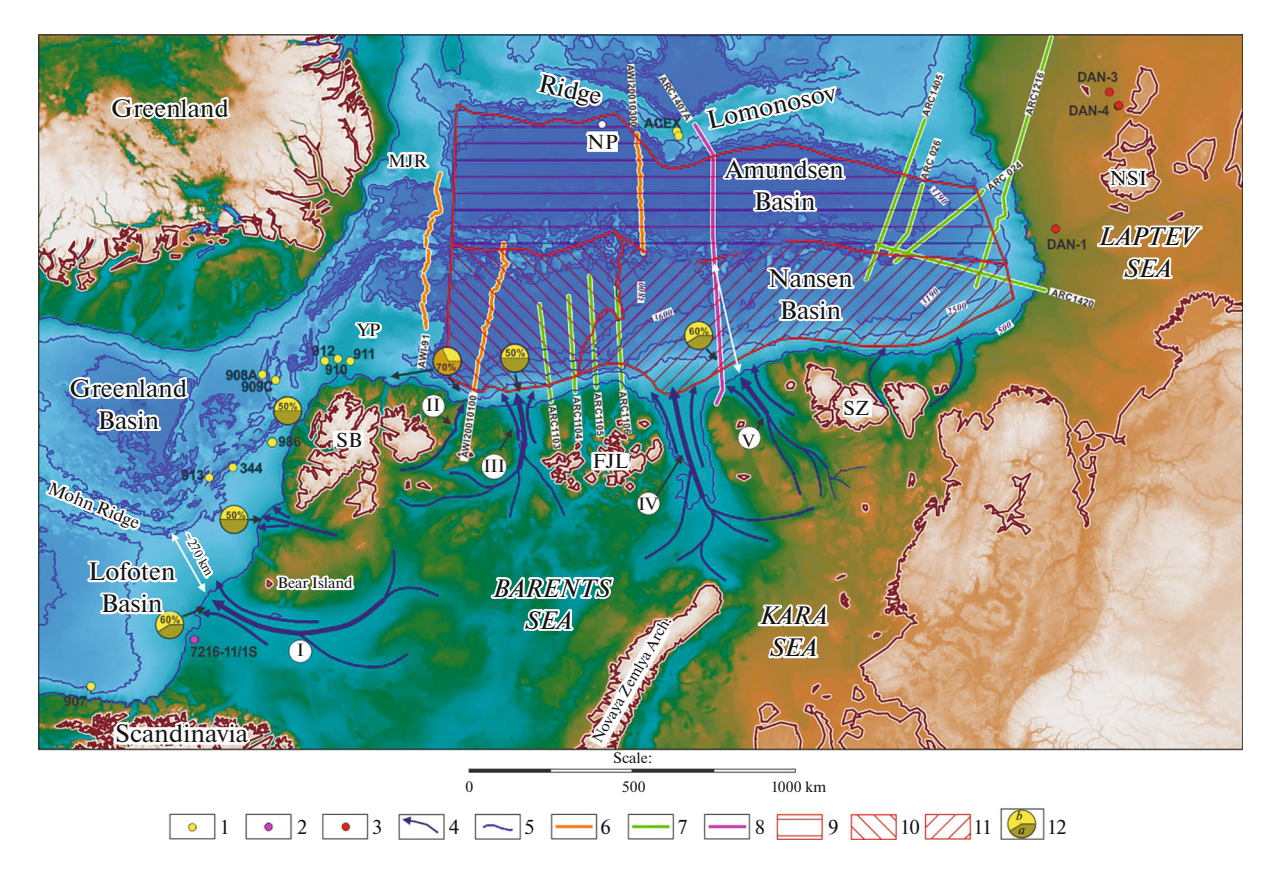


Fig. 1. Review scheme of the floor in the Eurasian and northern Norway—Greenland basins (Zayonchek et al., 2023) modified after (Alexandropoulou et al., 2021; Knies et al., 2009; Lasabuda et al., 2021; Malyshev, 2023; Zayonchek and Merkouriev, 2021). Based on the IBCAO digital model of the relief, v. 4 (Jackobson, 2020). Abbreviations: (NP) North Pole; (SB) Spitsbergen Archipelago; (FJL) Franz Josef Land Archipelago; (SZ) Severnaya Zemlya Archipelago; (NSI) New Siberian Islands; (YP) Yermak Plateau; (MJR) Morris Jesup Rise. (I) Bear Island Trough; (II) Orel Trough; (III) Franz Victoria Trench; (IV) Saint Anna Trench; (V) Voronin Trench. (1–3) Position of boreholes: (1) deep-water, (2) exploration, (3) shallow stratigraphic; (4) main directions of the transport of glaciomarine sediments; (5) isobaths 500, 2500, 3190, 3600, and 3800 m; (6–8) position of seismic profiles: (6) AWI (Germany), (7) ARC (Russia), (8) ARC1407A (Russia); (9–11) contours for the calculation of geomorphological characteristics: (9) Amundsen Basin, (10, 11) western and eastern parts of the Nansen Basin; (12) ratio of volumes of Cenozoic sedimentary rocks in the shelf-slope and deep-water basins: yellow color designates sediment age <~2.7 Ma (glaciomarine), pale brown, from ~57 to >~2.7 Ma (preglaciomarine).

detailed subdivision of glaciomarine deposits using the interpretation of seismic profile ARC1407A as example.

ANALYSIS OF PREVIOUS SEISMOSTRATIGRAPHIC CORRELATIONS OF GLACIOMARINE DEPOSITS

The correlation was performed for the southwestern Eurasian Basin and Norway—Greenland segment of the North Atlantic Ocean, which began to form in the Early Cenozoic (~55 Ma BP) due to pull-apart of the Eurasian and Greenland (North American starting from ~33 Ma) lithospheric plates (Engen, 2008; Faleide 1996; Gaina, 2002). The northern Norway—Greenland Basin accommodates the mid-oceanic Knipovich and Mohn ridges, which separate the Lofoten and Greenland basins (Fig. 1). Numerous seismic studies, starting from the western continental margin

of the Barents Sea toward the northern segment of the Mohn Ridge and the Knipovich Ridge, have recorded the presence of a thick sedimentary cover (up to ~6 km) overlying the crust of transitional and oceanic types on the continental slope and in the northeastern Norway—Greenland Basin (Alexandropoulou et al., 2021; Amundsen et al., 2011; Engen, 2009; Faleide et al., 1996; Fiedler and Faleide, 1996; Lasabuda et al., 2021). These rocks were recovered by deep-sea drilling and exploration boreholes on the western continental margin of the Barents Sea (Alexandropoulou et al., 2021; Butt et al., 2000; Channell et al., 1999; Eidvin and Nagy, 1999; Forsberg et al., 1999; Jansen et al., 1996; Geissler and Jokat, 2004; Knights et al., 2009; Myhre et al., 1995; Rebesco et al., 2014).

The seismostratigraphic analysis of Late Pliocene—Quaternary glaciomarine deposits (Fig. 2), which make up 30–60% of the total sedimentary cover thickness, allowed us to identify three seismic com-

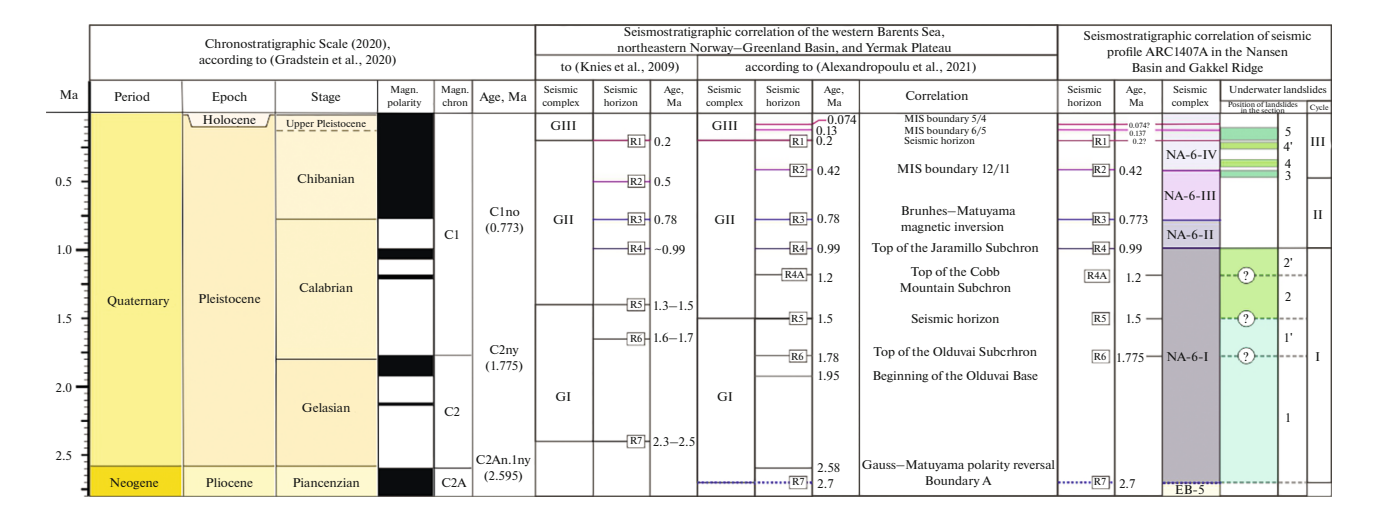


Fig. 2. Comparison of the seismostratigraphic correlation of glaciomarine deposits (since Late Pliocene) at the western margin of the Barents Sea and in adjacent areas of deep-water basins with the results of seismic profile ARC1407A interpretation. Compiled after (Alexandropoulou et al., 2021; Faleide 1996; Knies et al., 2009; Zayonchek et al., 2023). Based on the IBCAO digital model of relief, v. 4 (Jackobson, 2020).

plexes (Faleide et al., 1996; Fiedler and Faleide, 1996) reflecting the main phases of glacial erosion and sedimentation: GI (2.7–1.5 Ma), GII (1.5–0.2 Ma), and GIII (<0.2 Ma), based on the corrected age correlation in (Alexandropoulou et al., 2021).

Later, based on the analysis of clay minerals from the glacial debris (Knies et al., 2009) and 3D seismic exploration data (Laberg et al., 2010), researchers proposed models suggesting three main stages of ice sheet development in the Barents Sea in the Pliocene-Pleistocene (Figs. 3a–3b). The first stage was marked by the initial phase of ice sheet formation in the Late Pliocene-Early Pleistocene (~3.5-2.4 Ma BP). This period was likely limited by the coastline of mainland Norway in the southern area of the continental ice sheet. In the north, the ice cover occupied the Spitsbergen and Frantz Josef Land archipelagos and the spaces between them. In the east, it was located on the Novaya Zemlya Archipelago. During this period, channels (modern troughs and trenches on the Barents Sea shelf) promoted the large-scale transport of sediments on an ice-free continental slope (Andreassen et al., 2004; Laberg et al., 2010). At the second stage, the ice cover expanded in the Early and Middle Pleistocene (~2.4–1 Ma BP), resulting in the formation of the single Barents-Kara ice sheet. This is indicated by a gradual decrease in the amount of smectiterich sedimentary material delivered by the Siberian rivers due to the "blocking" of rivers by land ice (Knies et al., 2009). The development of a larger glaciation in the Early-Middle Pleistocene is also suggested by the regional 2D and detailed 3D seismic studies in the southwestern Barents Sea, suggesting glaciogenic mudflows on paleoslopes (Andreassen et al., 2007; Laberg et al., 2010), and by the evidence of large-scale movements along the western margin of the Barents Sea (Alexandropoulou et al., 2021; Faleide et al., 1996; Hjelstuen et al., 2007; Knies et al., 2009). At the final stage of the Middle Pleistocene (~0.8 Ma BP), the Barents–Kara ice sweet merged with the continental sheets synchronously with the global glaciation (Mudelsee and Stattegger, 1997) and a sea level drop by 20–30 m (Kitamura and Kawagoe, 2006).

The subsequent stratigraphic studies based on drilling results, including data on the Yermak Plateau (Alexandropoulou et al., 2021; Channell et al., 1999; Dessandier et al., 2021; Knies et al., 2009; Mattingsdal et al., 2014) and the interpretation of significant volumes of new 2D (Alexandropoulou et al., 2021; Knies et al., 2009) and 3D (Harishidayat et al., 2021) seismic data made it possible to identify additional reference horizons passing within seismic complexes (Fig. 2) and to refine the models of ice sheet development within the western Barents Sea (Figs. 3d-3f). The seismic studies clearly established the transport of sediments into the adjacent deepwater basin from the troughs located in the western Barents Sea. Intensity of the sedimentary material input allowed the glaciomarine sediments to reach the modern rift valley of Knipovich Ridge, where deposits up to 330 m thick were formed (Amundsen et al., 2011). The maximum transport into the Lofoten Basin was accomplished via the Bear Island Trough (Alexandropoulou et al., 2021; Faleide et al., 1996; Fiedler and Faleide, 1996; Lasabuda et al., 2021), which represented the most significant pathway within the Barents Sea (Figs. 1, 3). The modern Bear Island Trough is a transverse (relative to shelf) about 250 km wide trough formed as a result of numerous phases of ice flow movements and erosion in the Pleistocene (Batchelor and Dowdeswell, 2014; Vorren and Laberg, 1997). During periods of maximum ice cover expansion, ice flows from the

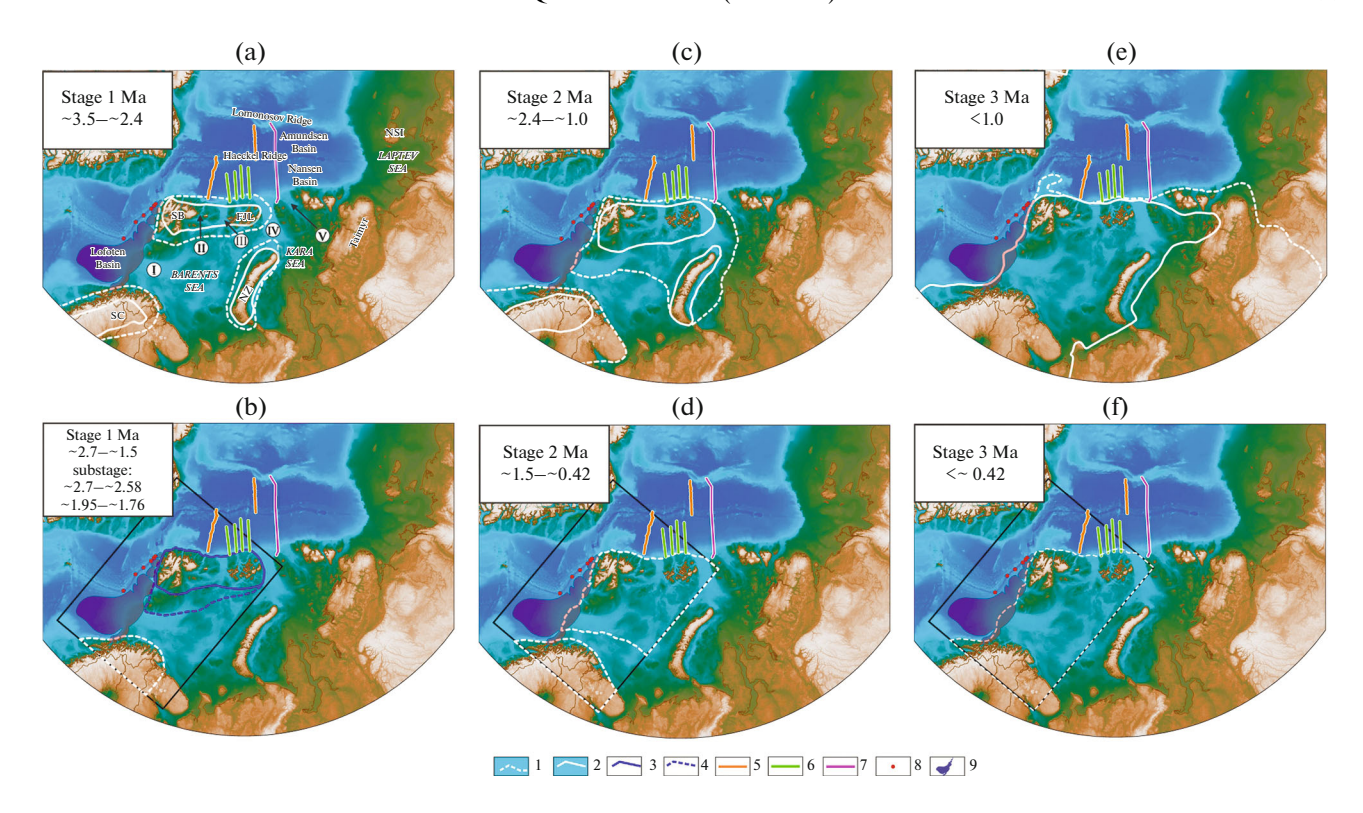


Fig. 3. Model of main stages of the development of ice sheet in the Barents Sea and adjacent areas since Late Pliocene. Based on the IBCAO digital model of relief, v. 4 (Jakobsson et al., 2020). Compiled after (Alexandropoulou et al., 2021; Amundsen et al., 2011; Bruvoll et al., 2009; Faleide, 1996; Gusev and Shkarubo, 2001; Knies et al., 2009; Safronova et al., 2017). (a, d) Stage 1: (a) ~3.5–2.4 Ma BP, according to Knies et al., 2009), (d) ~2.7–1.5 Ma BP, according to (Alexandropoulou et al., 2021); (b, e) stage 2: (b) ~2.4–1.0 Ma BP, according to Knies et al., 2009), (e) ~1.5–0.42 Ma BP, according to (Alexandropoulou et al., 2021); (c, f) stage 3 (c) <~1.0 Ma BP, according to (Knies et al., 2009), (f) <~0.42 Ma BP, according to (Alexandropoulou et al., 2021). Abbreviations: (SC) Scandinavia; (SB) Spitsbergen Archipelago; (FJL) Franz Josef Land Archipelago; (SZ)Severnaya Zemlya Archipelago; (NZ) Novaya Zemlya Archipelago, (NSI) New Siberian Islands. (I) Bear Island Trough; (II) Orel Trough; (III) Franz Victoria Trench; (IV) Saint Anna Trench; (V) Voronin Trench. (1) Terrain of the maximum ice sheet development; (2) terrain of the minimum ice sheet development; (3, 4) terrain of the maximum ice sheet development during (Ma BP): (3) ~2.7 to ~2.58, (4) ~1.95 to 1.5; (5–7) position of seismic profiles: (5) AWI (Germany), (6) ARC (Russia), (7) ARC1407A (Russia); (8, 9) terrain of glaciomarine deposits: (8) based on seismic data on rift valleys in the Knipovich and Mohn Ridges, according to (Amundsen et al., 2011; Bruvoll et al., 2009; Gusev and Shkarubo, 2001); (9) contour of Pliocene—Pleistocene landfalls in the northeastern Norway—Greenland Basin (semi-transparent shading), according to (Safronova et al., 2017).

Bear Island Ice Stream transported significant volumes of deformed subglacial sediments to the shelf edge, which were deposited in the upper part of the continental slope as lobe sediments or "glacial debris flows" (Andreassen et al., 2007; Laberg et al., 2010; Safronova et al., 2017). The accumulation of this material led to the development of a large glacial-sedimentary depocenter or estuarine Bear Island Trough Fan (Vorrena and Laberg, 1997; Waage et al., 2018). The Bear Island Trough Fan (about 350,000 km³) is one of the largest trough fans in the world (Batchelor and Dowdeswell, 2014). The sediments and morphologies, retained in this depocenter, indicate glacial processes in the southwestern Barents Sea during the Ouaternary.

Intensity of the transport was so significant that glaciomarine deposits reached the northern Mohn Ridge (Bruvoll et al., 2009), located about 220 km from the Bear Island Trough mouth (Figs. 1, 3). On

the southwestern wall of the trough, an exploration borehole 7216/11-1S (sea depth 361 m) was drilled and a significant amount of 3D seismic exploration was accomplished (Harishidayat et al., 2021; Laberg et al., 2010; Waage et al., 2018). In the sampling interval, biostratigraphic methods have established that the Pliocene/Pleistocene boundary, located at 1500-1600 mbsf (Knies et al., 2009), is recognized on the seismic record as a reflection at ~1.76 s (two-way traveltime of indicated seismic reflection hereinafter). The boundary of the glaciomarine stage beginning (Fig. 2, R7 2.7 Ma BP) has not been established directly by biostratigraphic methods in this borehole. However, based on the seismic correlation, the boundary is identified as a reference horizon at ~2.2 s; i.e., total thickness of sediments younger than 2.7 Ma is ~1800 m.

The transitional Barents/Kara boundary area accommodates the Saint Anna Trough, which is comparable in scale to the Bear Island Trough. Therefore,

we assume that the observed local rise on the continental slope, located opposite the trough, is related to the transport of significant volumes of glaciomarine sediments (Faleide et al., 1996; Lasabuda et al., 2021; Medvedev et al., 2023). Interpretation of seismic profile ARC1407A, located near the Saint Anna Trough mouth opposite the western Voronin Trough, confirmed this assumption (Zayonchek et al., 2023) and revealed that the glaciomarine sediments near the continental margin, as well as opposite the Bear Island Trough, can reach ~60% of the total sedimentary cover thickness (Fig. 1).

INITIAL DATA

We used the International Bathymetric Chart of the Arctic Ocean, Version 4.0, resolution 200×200 m (Jakobson et al., 2020) (without the Greenland ice sheet) as a bathymetric basis. The data used for compiling the digital model (DM) of the Eurasian Basin is analyzed in (Zayonchek et al., 2023). The above work also presents calculations of the theoretical position of linear anomaly axes, theoretical age of the oceanic crust, and results of the seismic profile ARC1407A interpretation.

GEOMORPHOLOGICAL ANALYSIS

The fan-shaped apron of glaciomarine sedimentary material transported from troughs in the western Barents Sea is clearly expressed in the elevation of the bottom relief (Fig. 1). In the Eurasian Basin, which is divided into two basins by the mid-oceanic Gakkel Ridge, a similar elevation is recorded in the Nansen Basin and in the Laptev Sea part of the Amundsen Basin (Fig. 1). The Eurasian Basin has a prominent wedge-shaped morphology that narrows toward the continental margin of the Laptev Sea due to poles of the opening of the Eurasian and North American plates located close to the coast (Glebovsky et al., 2006; Merkouriev, 2014). An exception to the general narrowing of the Eurasian Basin toward the continental margin of the Laptev Sea is observed only in the westernmost narrow, Morris Jesup Rise/Yermak Plateau segment, which began to open much later (Glebovsky et al., 2006; Zayonchek et al., 2023). The basin width is ~650 km opposite the Spitsbergen Archipelago, ~650 km along seismic profile ARC1407A, and ~530 km opposite the Severnaya Zemlya Archipelago.

One of the most striking features of the Eurasian Basin is the depth asymmetry of the bottom of deepsea basins (Fig. 1). The intermontane depressions in cis-rift mountains of the Gakkel Ridge in the central and eastern parts of the basin are covered by a thick sedimentary cover that also extends into the rift valley noted in the seismic record (Jokat and Micksch, 2004; Nikishin et al., 2018; Zayonchek et al., 2023). Therefore, when studying the whole area rather than individual seismic profiles, there is some uncertainty in

identifying the boundaries separating the ridges and basins, and it is impossible to accomplish a rigorous statistical analysis of comparisons of the basin depth.

Therefore, it is logical to draw the boundary along the modern opening axis—center of the Gakkel Ridge rift valley. In this case, identification of the Amundsen and Nansen basins will be conditional, since the cisrift mountains and a part of the Gakkel Ridge rift valley will fall into the basins, but this is not essential for the comparative statistical analysis because of the following reasons:

- since the opening axis runs approximately along the rift valley center, one of its walls will be taken into account in assessing the Amundsen Basin relief and the second wall be included in the Nansen basin, creating a balancing influence on the statistics;
- on the contrary, discrepancy in the thickness of sediments in the cis-rift parts of the basins will be manifested, resulting in statistically different values of the basement depth.

Quite often, during regional studies, the opening axis is drawn along the axis of the minimum free air gravity anomalies in the above the rift valley. We gave priority to the IBCAO v.4 relief data supplemented with the multibeam echosounder data (except for the easternmost section). Compilations of gravity anomalies for the Arctic were smoothed (Zayonchek et al., 2023). For areas with minor displacements of the rift valley and for the easternmost part of the Eurasian Basin, preference was given to gravity anomalies according to the WGM-2012 project data (Bonvalot et al., 2012). The position of the continent—ocean boundary (COB) from the Barents—Kara margin and Lomonosov Ridge was determined by gravity field anomalies (Zayonchek et al., 2023).

Such a definition of COB, especially in areas with smoothed relief of the continental margins, is rather arbitrary, but it allowed us to outline contours as a first approximation the conditional Amundsen and Nansen basins (Fig. 1), within which the statistical calculations were accomplished. The results, presented as bar charts (Fig. 4), show discrepancies in the depths and nature of their distribution. For the Amundsen Basin, the average depth of 4010 m is clearly recorded as a single peak in the region of 4320 m against the background of a regional lowering of relief in the range of 4180–4380 m (Fig. 4a). For the Nansen Basin as a whole, the average depth is 3360 m, which is 650 m less than for the Amundsen Basin. In the deep-sea part, between 3780 and 4020 m, the bar chart shows three local peaks and two distinct narrow peaks at 3190 and 3600 m (Fig. 4b), indicating an internal asymmetry of depths. In the central Nansen Basin, the boundarv of its western and eastern regions is quite clearly recorded by the submeridional segment of isobath 3800 m (Fig. 1). For the western Nansen Basin, the average depth is 3715 m, and the range of 3800–4020 m includes two peaks at 3860 and 4000 m (Fig. 4c). In

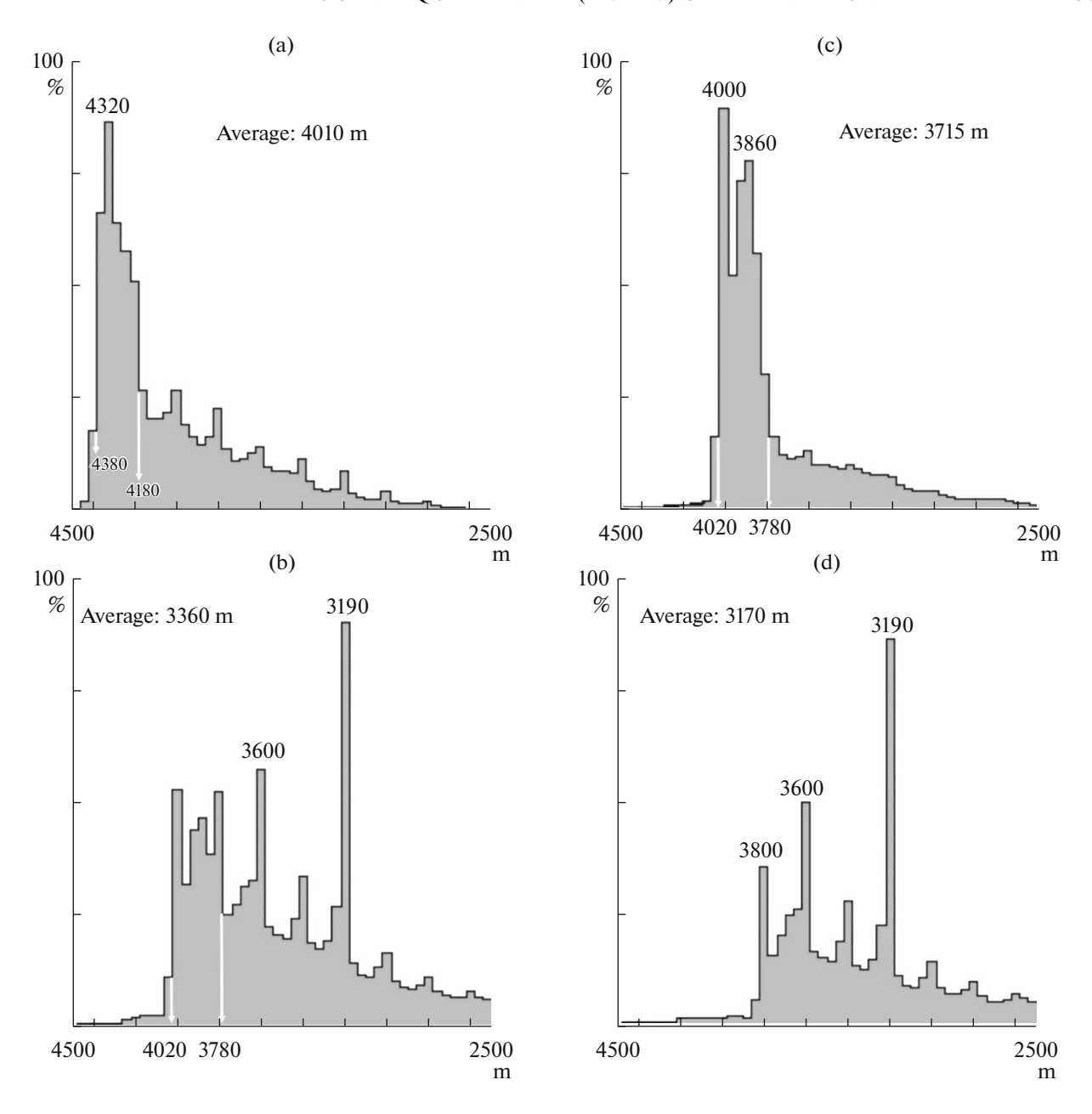


Fig. 4. Bar charts of depths in the Eurasian Basin (calculation contours are given in Fig. 1). (a) Nansen Basin, (b) Amundsen Basin, (c) eastern Nansen Basin, (d) western Nansen Basin. Calculations are based on the matrix of IBCAO v.4.0 (Jakobsson et al., 2020).

the Nansen Basin, the average depth is 3170 m and three peaks (3190, 3600, and 3800 m) are recorded (Fig. 4d). A visual analysis of the identified statistical peaks (Fig. 1) suggests the following conclusions.

1. The 3800-m isobath delineates the Gakkel Ridge rift valley approximately up to seismic profile ARC 024, which records a sufficiently thick sedimentary cover within the rift valley (Nikishin et al., 2018). In the Amundsen Basin, the 3800-m isobath records its deep-water part. It is separated by cis-rift mountains of the Gakkel Ridge from the south and by the Lomonosov Ridge foothill in the north. In the western

Nansen Basin, a similar pattern of separation of the deepwater part from the rift is observed, but the continental slope is significantly gentler than in the Amundsen Basin on the Lomonosov Ridge side and much longer.

2. The 3600-m isobath actually divides the eastern Nansen Basin into two parts: the deepwater one lying between isobaths 3600–3820 m, and the offshore part lying between isobaths 3190–3600 m. In the eastern Nansen Basin, individual peaks of the cis-rift mountains form local and narrow chains extending along the

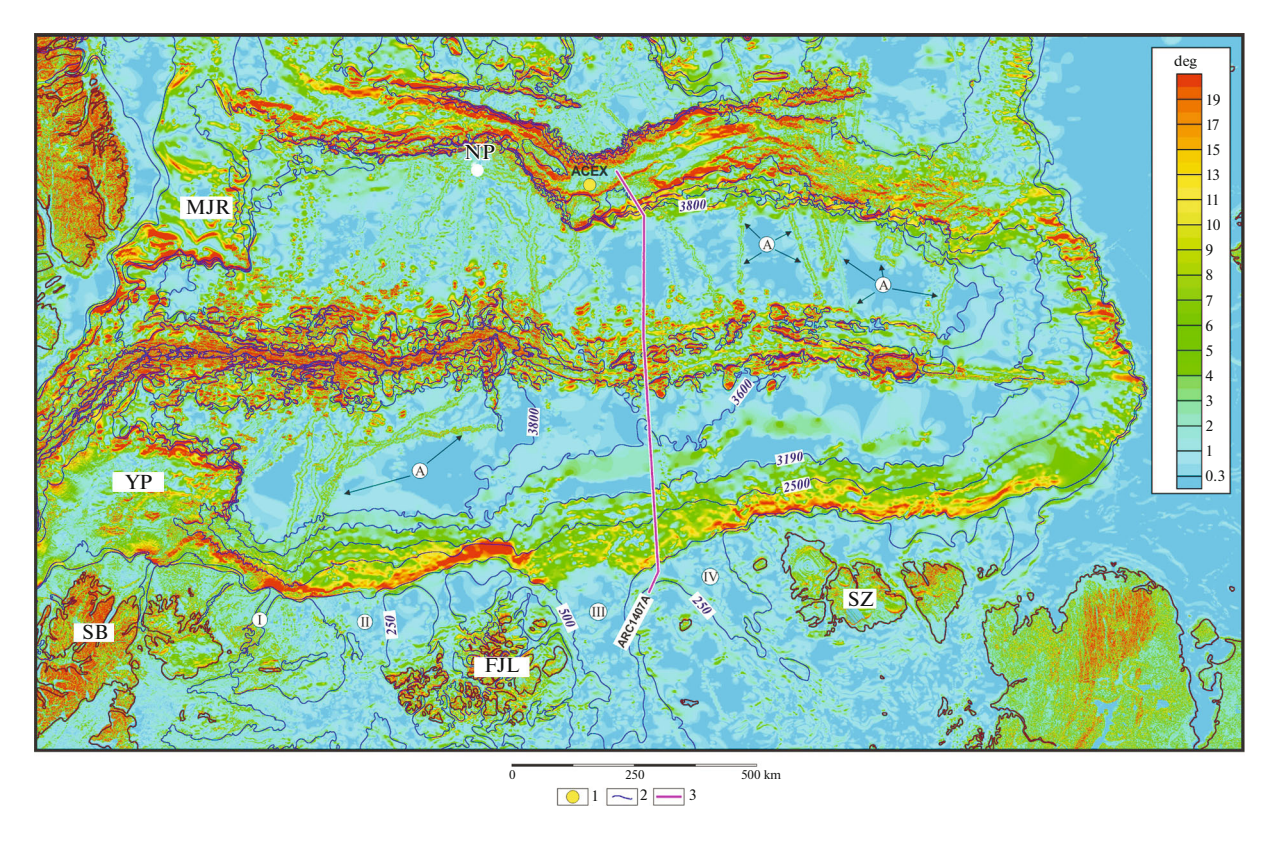


Fig. 5. Schematic slope angles in the Eurasian Basin and adjacent areas of the shelf, continental slope, and Lomonosov Ridge. Calculations are based on IBCAO v.4.0 values (Jakobsson et al., 2020). Abbreviations as in Fig. 1: (NP) North Pole; (SB) Spitsbergen Archipelago; (FJL) Franz Josef Land Archipelago; (SZ) Severnaya Zemlya Archipelago; (YP) Yermak Plateau; (MJ) Morris Jesup Rise; (A) artefacts. (I) Orel Trough; (II) Franz Victoria Trough; (III) Saint Anna Trough; (IV) Voronin Trough. (1) Position of borehole ACEX; (2) isobaths 250, 500, 2500, 3190, 3600, and 3800 m; (2) position of seismic profile ARC1407A (Russia).

rift valley, indicating the filling of intermontane depressions with sediments.

The slope angles suggest the division of the Barents-Kara continental slope into several segments and its significant continuation into the Nansen Basin (Fig. 5). The western segment (between the eastern Spitsbergen Archipelago and Franz Josef Land Archipelago) is characterized in the upper part of the slope by significant slope angles (>15°), which decrease slightly opposite the Franz Victoria Trench marked by the formation of several terraces. Opposite the Saint Anna and Voronin troughs, the slope angle decreases (maximum 11°). After a series of terraces, the farthest slope portion in the northern direction with average slope angles of $\sim 2^{\circ}-3^{\circ}$ (up to 3600-m isobaths) is located already in a deep-water basin. From the eastern end of the Voronin Trench to the beginning of the Laptev Sea slope, the slope angle increases at the beginning and a series of terraces are recorded in the northern direction.

In the Amundsen Basin, slope angles record the Lomonosov Ridge slope and suggest a system of underwater canyons roughly perpendicular to the Laptev Sea continental margin.

One of the basic elements of geomorphological slope analysis is the calculation of the LS factor, which is a combination of the slope angle and its length. Since the IBCAO v. 4 digital model is a compilation of completely different data sets (Zayonchek et al., 2023), we limited our calculations to using one of the basic methods described in (Moore and Neiber, 1989). The calculation results (Fig. 6) establish the continuation of the underwater canyon systems starting on the slope and continuing into the deep-water part of basins. The figure shows an "overlap" of two directions north of the Franz Victoria Trough. The first northern direction starts from the continental slope edge, approximately corresponding to the 500-m isobath, continues on the slope and in the deep-sea basin (depth >3190 m). In the eastern part, opposite the Franz Josef Land Archipelago, this direction is "truncated" by another underwater canyon system, which shows a northwestward direction and begins in the deep part as the western continuation of the system opposite the Saint Anna and Voronin troughs. Directly in the center of the Saint Anna Trough, the system can be traced back to the cis-rift mountains and has a length of about 400 km (Fig. 6).

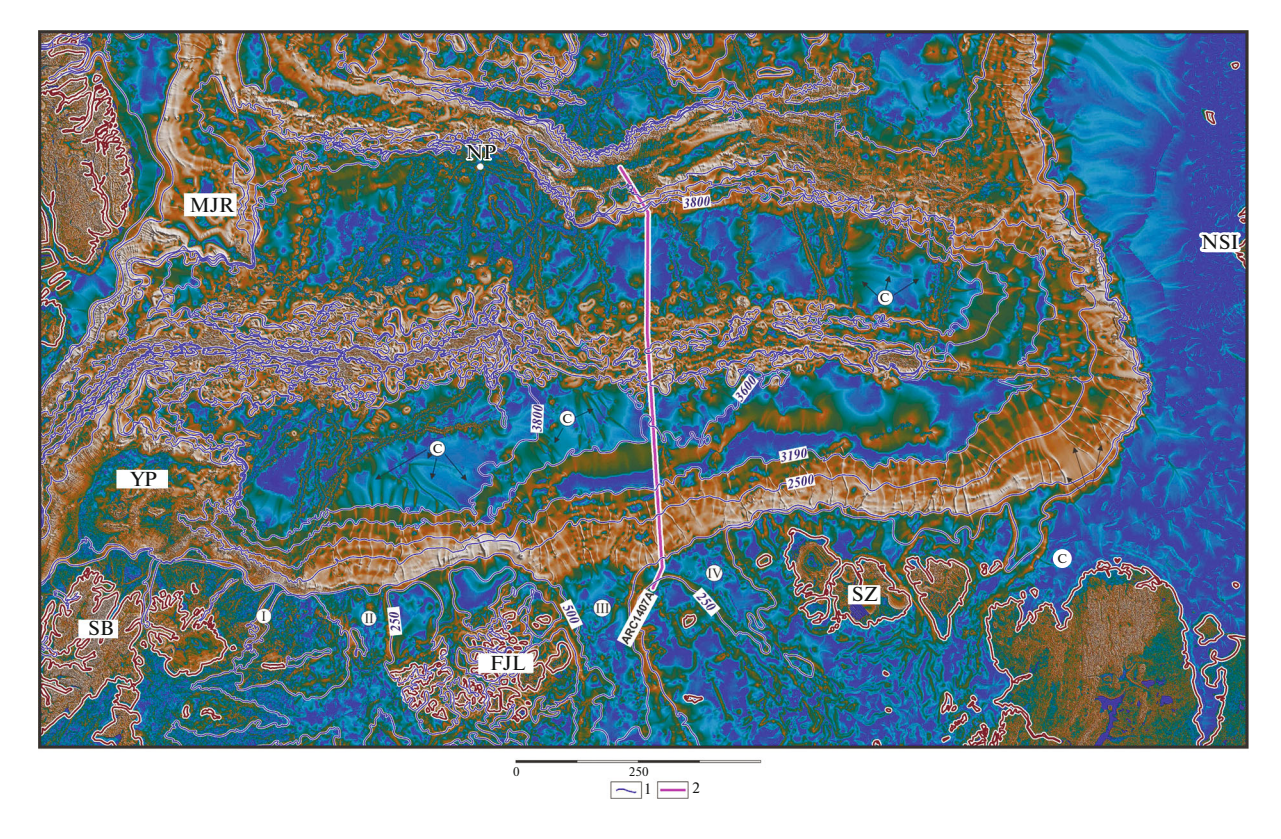


Fig. 6. Relationship of slope angles and slope lengths (LS-Factor) in the Eurasian Basin and adjacent areas of the shelf, continental slope, and Lomonosov Ridge (psudoshadow presentation. Backlight angle 45 degr). Calculations are based on the matrix of IBCAO v.4.0 values (Jakobsson et al., 2020). Abbreviations: (NP) North Pole; (SB) Spitsbergen Archipelago; (FJL) Franz Josef Land Archipelago; (SZ) Severnaya Zemlya Archipelago; (NSI) New Siberian Islands; (YP) Yermak Plateau; (MJ) Morris Jesup Rise; (C) canyons. (I) Orel Trough; (II) Franz Victoria Trough; (III) Saint Anna Trough; (IV) Voronin Trough. (1) Isobaths 250, 500, 2500, 3190, 3600, and 3800 m; (2) position of seismic profile ARC1407A (Russia).

A different arrangement of canyon systems is observed in eastern parts of the Nansen and Amundsen basins. On the western Laptev Sea continental slope toward the Nansen Basin, a well-developed system of underwater canyons is traced clearly from the continental slope, located at depths of <500 m, to isobaths of 3190 m. On the western Laptev Sea continental slope toward the Amundsen Basin (AM), the underwater canyon system is not so obvious, but it crosses the 3190-m isobath and is clearly traced westward in the deep-water basin. The distance from the slope edge to its disappearance site is approximately 600 km (Fig. 6).

In (Rekant et al., 2020), based on small slope angles, the mechanism of large-scale transport of terrigenous sediments from continental margins of the Barents–Kara and Laptev Sea into the deep-water basin is denied. Instead, the presence of thick sedimentary rocks is explained by the pelagic type of sedimentation in the Eurasian Basin. The distance from the Voronin trough center to the central Gakkel Ridge, where thick sedimentary rocks are recorded in the rift valley, is ~370 km. (Fig. 1). The underwater canyon system continues up to the cis-rift mountains (Fig. 6). In the eastern Amundsen Basin, the domain of sedi-

ment input from the Laptev Sea continental margin is limited to a distance of 70 km (Rekant et al., 2021), which is about 8.5 times less than the length of the modern underwater canyon system (Fig. 6).

The geomorphological analysis revealed a significant input of sediments from the Barents—Kara margin into the Nansen Basin and from the Laptev Sea into the eastern Amundsen Basin.

SEISMOSTRATIGRAPHIC CORRELATION OF GLACIOMARINE DEPOSITS (<2.7 Ma) AND ARC1407A SEISMIC PROFILE

If boreholes are lacking, the seismostratigraphic correlation of the sedimentary cover in spreading basins is based on the following principle: sediments older than those in the underlying oceanic crust cannot be formed. This principle was used widely for determining the age of sedimentary sequences in the Eurasian Basin by identifying the overlap points (closest to the rift valley) of the reference reflecting horizons (RH) on the oceanic basement. The basement age was based on results of the identification of axes of linear magnetic anomalies (Engen, 2009; Nikishin et al., 2018) or calculations of the theoretical age of the

Magnetic chrons	Age, Ma	Opening poles		Half angular	Seismostratigrap	Note
		latitude, deg	longitude, deg	opening	hic reference	Note
	0.2				R1	
	0.42				R2	Linear interpretation
1no	0.773	-60.32	320.4	0.0790	R3	
	0.99				R4	Linear interpretation
	1.5				R5	Linear interpretation
2ny	1.775	-63.65	315.8	0.1815	R6	
2An.1y	2.595	-63.81	318.16	0.2690		
	2.7				R7	Linear interpretation
2An.3o	3.596	-62.94	319.02	0.3720		
3n.1y	4.187	-62.38	317.91	0.4290		

Table 1. Position of poles of the half angular opening of the North American and Eurasian plates, according to (Merkouriev and De Mets, 2014)

End of chrons—(y) young, beginning of chrons—o. The half angular opening was obtained by the twofold reduction of opening angles. Seismostratigraphic correlation and indexation of RH, according to (Alexandropoulou et al., 2021; Faleide et al., 1996). Age, according to the GTS2020 geochronological scale (Gradstein et al., 2020).

oceanic basement (Zayonchek et al., 2023). The Eurasian Basin is provided with only a few seismic profiles starting from the continental margin and crossing or ending in the Gakkel Ridge rift valley (Fig. 1). Unfortunately, in the central part of the basin, seismic profiles are laid out in such a way that they intersect the rift mountains on the ridge, and do not pass over intermontane depressions, hampering a direct correlation of the RHs or their portions from the basins the rift valley of the ridge.

Theoretical calculations of the oceanic crust age remain the only correlation method in such case. In (Amundsen et al., 2011), results of the seismostratigraphic correlation of glaciomarine deposits in the Knipovich Ridge rift valley, which reached this area during the main stages of transport from the shelf zone (GI, GII, and GIII, Fig. 1), were compared with theoretical calculations of the oceanic crust age based on the average half-rate of the Knipovich Ridge opening. In the present work, calculations of the theoretical position of the axes of linear anomalies (TLMA) were based on the position of rotation poles of the North American and Eurasian plates and the opening angles adopted from (Merkouriev, 2014) (Table 1).

The seismostratigraphic correlation of seismic profile ARC1407A is shown in Figs. 7a, 7b, and Appendix 1. The position of TLMA and the corresponding age are shown above the seismic section. For the convenience of comparison, the general indexing of seismic complexes is adopted from (Zayonchek et al., 2023).

The position of the modern spreading center, relative to which the calculations were carried out, is borrowed from (Zayonchek et al., 2023) showing a local rise, which can be identified as neovolcano based on the seismic record, at the rift valley center rise. The age of some RHs, determined for the western and north-

western margins of the Barents Sea and adjacent deepsea basins (Fig. 2), does not fit the boundaries of the magnetic polarity chrons. Therefore, points of the theoretical oceanic crust age (~0.42 (R2), ~0.99 (R4), and ~2.7 (R7) Ma) were determined by the linear interpolation. The position of TLMA (Fig. 7a) and their age older than Chron 3An.1y (~6 Ma) is adopted from (Zayonchek et al., 2023). The position of TLMA and their age younger than Chron 3An.1y (~6 Ma) are determined in the present work (Fig. 7b, Appendix 1).

If we accept results of the seismostratigraphic correlation of glaciomarine deposits in the northeastern Norway—Greenland Basin (Fig. 2), the age of a part of RH identified within the Gakkel Ridge rift valley (Fig. 7b) fits the boundaries of reflecting horizons R1 (~0.2 Ma), R2 (~0.42 Ma), R3 (~0.773 Ma), and R4 (~0.99 Ma). Therefore, we denoted the sedimentary seismic complexes bounded by RH surfaces as NA-7-I, NA-7-II, NA-7-III, and NA-7-IV—(NA) Nansen Basin, (7) the sequence level, according to (Zayonchek et al., 2023), (I—IV) indexation of the seismic complex. Additional RHs are identified within the seismic complex, but their stratigraphic correlation is uncertain.

- 1. Within the central part of the rift valley, the uppermost seismic complex NA-7-IV (<~0.42 Ma) directly overlies the oceanic basement portion F1 (Fig. 7b, Appendix 1). Therefore, the RH identified within this part cannot be correlated seismostratigraphically by the applied methodology.
- 2. The seismic section within the upper summary seismic complexes NA-7 (Nansen Basin and AM-6 (Amundsen Basin) differs markedly (Fig. 7a). The Nansen Basin includes significant areas marked by loss or partial loss of signal coherence interpreted as landslide bodies or intense turbidite flows (Engen et al., 2009; Sokolov et al., 2021; Zayonchek et al.,

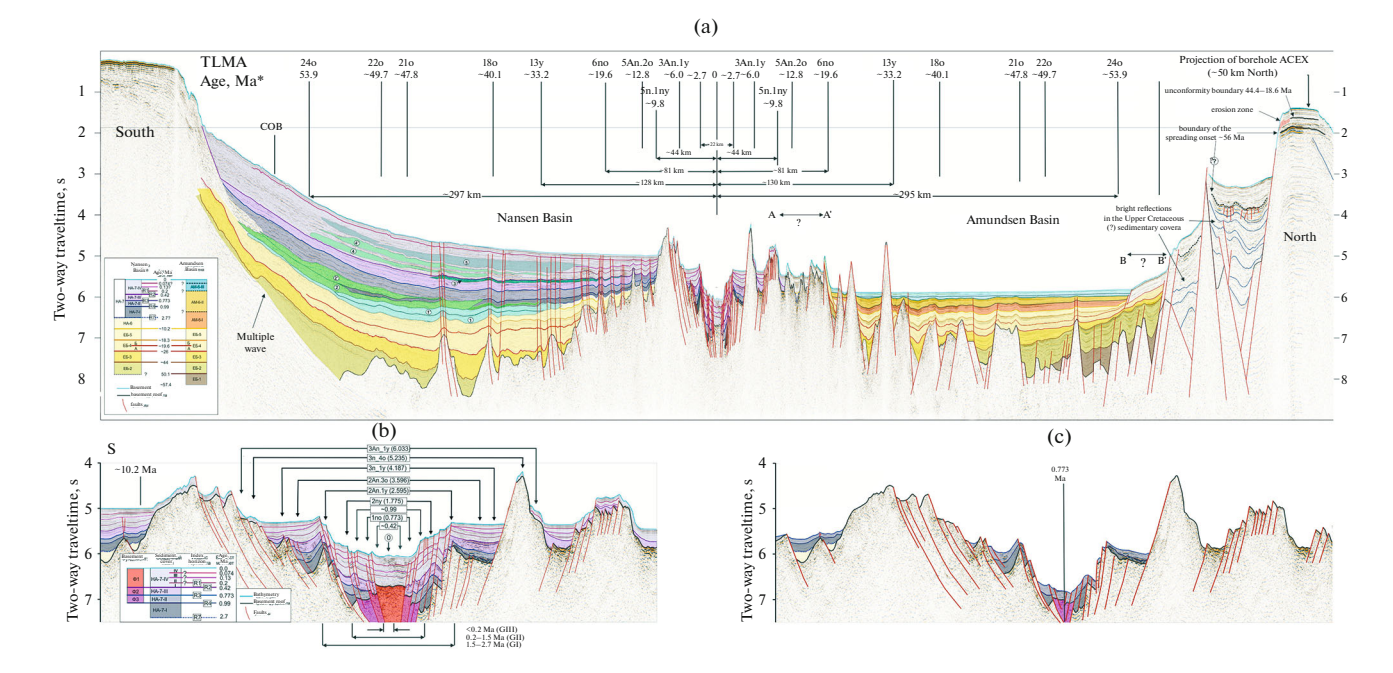


Fig. 7. Seismostratigraphic interpretation of the ARC1407A seismic time section. (a) Complete section; (b) closeup of the central part of section; (c) reconstruction of the central part of the section for the theoretical age of the oceanic crust (\sim 0.773 Ma). (A–A', B–B') uncertainty range of tracking regional stages in the upper part of the sedimentary cover. Coherence signal loss zones (submarine landslides) formed during various sedimentation cycles (Fig. 2): (1,1' and 2,2') cycle I, (3) cycle II, (4,4 and 5) cycle III. Abbreviations: (TLMA) theoretical position of linear magnetic anomalies on the profile.

2023). On the northern flank of Gakkel Ridge, one can see an uncertainty zone (A–A') of the RH correlation due to a rugged pattern of the basement surface—see (Zayonchek et al., 2023) for more detail. In the Amundsen Basin, the reflection pattern is generally quite clear, and the sedimentary cover with an age of <10.2 Ma can be divided conditionally into three seismic complexes—AM-6-I, AM-6-II, and AM-6-III (Fig. 7a, Appendix 1) marked by a slight loss of signal coherence

3. The cis-rift protrusions hamper the continuous RH tracing.

Because of the applied seismostratigraphic correlation method and the above-described uncertainties, it is logical to identify the regularities of sedimentation within the rift valley (center—0 Ma) and its nearest flanks (Fig. 7b, Appendix 1). In this area, based on the seismic record pattern, seismic complex NA-7-IV (base R2, ~0.42 Ma, MIS 12/11) is divided by the characteristic RHs into four seismic packages (NA-7-IV-I, NA-7-IV-II, NA-7-IV-III, and NA-7-IV-IV).

It is logical to assume that three RHs separating the seismic complex correlate with the boundaries of R1 (~0.2 Ma), MIS 6/5 (~0.13 Ma), and MIS 5/4 (~0.073 Ma) (Figs. 2, 7b, Appendix 1). Specific features of the relationship between these three RHs are very clearly manifested within the ridge flanks in the theoretical age region (~2.595 Ma) of the oceanic crust (from walls of the rift valley to the cis-rift mountains).

Within the two lower seismic blocks (NA-7-IV-I and NA-7-IV-II), the reflecting horizons are clearly parallel, and their shape repeats the reflection inside the underlying NA-7-III seismic complex. Thickness of the overlying seismic package (NA-7-IV-III) decreases gradually from the cis-rift mountains toward the uplifted flanks of the rift valley up to the point of pinchout, which is unobserved in the uppermost seismic package (NA-7-IV-IV). At the same time, the southern flank records a reflection angle flattening as compared to those observed in the underlying seismic packages, suggesting that the sediments were formed at various geodynamic development stages of the rift valley and its proximal flanks.

The following scenario can be proposed for the upper seismic complex NA-7-IV formation. The Gakkel Ridge (oceanic crust portion younger than ~20 Ma (Glebovsky, 2006)) belongs to a super-slow spreading area, i.e., characterized by impulsive opening when the tectonic lull stage is replaced by the tectonomagmatic activation stage. The three lower seismic complexes (NA-7-IV-I, NA-7-IV-II, and NA-7-IV-III) appeared rather quickly during the tectonic lull, which began ~0.42 Ma BP and was characterized by the absence of significant extension in this segment, as evidenced by the constancy of thicknesses within the rift valley. In the northern part of the rift valley, contrasting reflections are distinguished within these seismic complexes, which can be interpreted as the intrusion of basalts and the beginning of activation phase, resulting in uplift of the rift valley walls and the consequent erosion of the NA-7-IV-III seismic block and local redeposition of unconsolidated sediments, probably, due to intensification of seismicity. The sediments were transported toward the rift valley, resulting in thickening of this seismic package. The uppermost seismic package (NA-7-IV-IV) was formed with a time lag followed by intensification of the tectonomagmatic activation.

The rift valley center within this seismic package was marked by an intensification of reflections and a partial loss of correlation, probably, due to modern intrusion of basalts into the sedimentary cover as sills and dikes (with the sedimentary cover deformation) and the appearance of central local rise as a neovolcano. In this part of the seismic profile, two sonobuoy stations were deployed (Nikishin et al., 2018). The seismic velocity was 1.6 km/s in the topmost parts of the section and 1.9 km/s in the middle part. Increased velocities (2.5–2.7 km/s) in the lower part of the section can represent the basalt intrusion into the sediments.

The current and recent magmatic activation in this segment of the Gakkel Ridge is confirmed indirectly by the discovery of two rises and a separate seamount within its rift valley (Michael et al., 2003) in the segment located to the west. This area ("85°E") was mapped during the multi-beam echosounder survey (project AGAVE-2007) that discovered three conical volcanoes with signs of modern and recent eruptions (Oden, Thor, and Loke) within the axial part of the rift valley (Pontbriand et al., 2012). The volcanoes are located near the axial volcanic ridges (Jessica's Hill and Duque's Hill). Detailed photographs of the seabed record the presence of numerous small lava flows of various ages and morphologies within the axial valley, as well as friable volcaniclastic sediments up to 10 cm thick. Lava flows, apparently, erupted from several separate sources in the axial valley 12–15 km wide.

The underlying seismic complex NA-7-III ($\sim 0.42-0.773$ Ma), whose base is limited by RH R3, generally follows the geometry of the lower part of the overlying seismic complex, but is characterized by the presence of contrasting reflections, probably indicating magmatic activation during its formation. The simplest juxtaposition of the seismic section on the age of ~ 0.773 Ma BP, when the seismic complex began to form theoretically (Fig. 7c, Appendix 1), shows a good coincidence of RH within the rift valley and elevated flanks, but its absence in the intermontane depressions of syn-rift mountains in the Amundsen Basin.

The underlying seismic complex NA-7-II (~0.773–0.99 Ma), whose base is limited by R4 RH, mimics the geometry of the overlying seismic complex and is characterized by the presence of contrasting reflections. The contrast range of reflections is slightly lower, which is most likely related to the beginning of intense attenuation of the seismic signal. The seismic

complex is slightly thicker on ridge flanks on the Nansen Basin side, relative to the opposite side in the Amundsen basin (Figs. 7b, 7c, Appendix 1).

On the flanks and walls of the rift valley, the lower seismic complex (NA-7-I, >~0.99 Ma) lies on the oceanic basement and is characterized by several specific features (Figs. 2, 7b, Appendix 1). Based on theoretical calculations, the age of its appearance in the rift valley is ~1.775 Ma, which corresponds to boundary R6, according to (Alexandropoulou et al., 2021). On the flank toward the Amundsen Basin, the seismic complex is significantly thinner than on the symmetrical flank toward the Nansen Basin.

Based on theoretical calculations, the central part of the rift valley (F1, Fig. 7b) was formed during <0.42 Ma. Thickness of seismic complex NA-7-IV is ~0.7 s, corresponding to a thickness of ~630 m at an average sedimentation rate of 1.8 km/s. Then, average sedimentation rate is 1.5 km/Ma, which looks excessive for the pelagic type of sedimentation. The "instantaneous" accumulation of a thick sedimentary shell in the rift valley due to intense landslide and turbidite flows from the continental margin troughs seems to be a more plausible scenario, which is established for the northeastern Norway—Greenland Basin described above.

DISCUSSION

The Bear Island Trough Fan extends from the modern continental slope edge toward the deepwater basin over about 620 km (Fig. 3), which is significantly more than the distance from the continental slope edge to the Gakkel Ridge rift valley (~370 km) along seismic profile ARC1407A (Fig. 7a) and is comparable to the distance from the modern Bear Island Trough edge to the northern portion of the Mohn Ridge marked by glaciomarine deposits. The sporadic development of sediments with an age of <2.7 Ma in the Knipovich Ridge rift valley is explained by the blocking of landslide and turbidite flows from troughs at the western margin of the Barents Sea by the rift mountains. The flows pass around the seamounts and enter the valley only through intermontane depressions.

Such sediment formation mechanism seems to be valid for the central and, partially, eastern parts of the Gakkel Ridge rift valley. The slope angles (Fig. 5) indicate the following scenario: upon approaching the rift valley from the Nansen Basin, seismic profile ARC1407A crosses the edge of local syn-rift mountains and then approaches a relief depression (intermontane depression) in the west in the axial part of the rift.

We can assume the following scenario for the cyclical formation of Late Pliocene—Quaternary glaciomarine deposits in the Eurasian Basin. The Saint Anna Trench is slightly smaller than the Bear Island Trough, as evidenced by its large area within the 500-m isobath (Fig. 1). Similarly as the Bear Island Trough, the Saint Anna Trough served during the Late Pliocene—Qua-

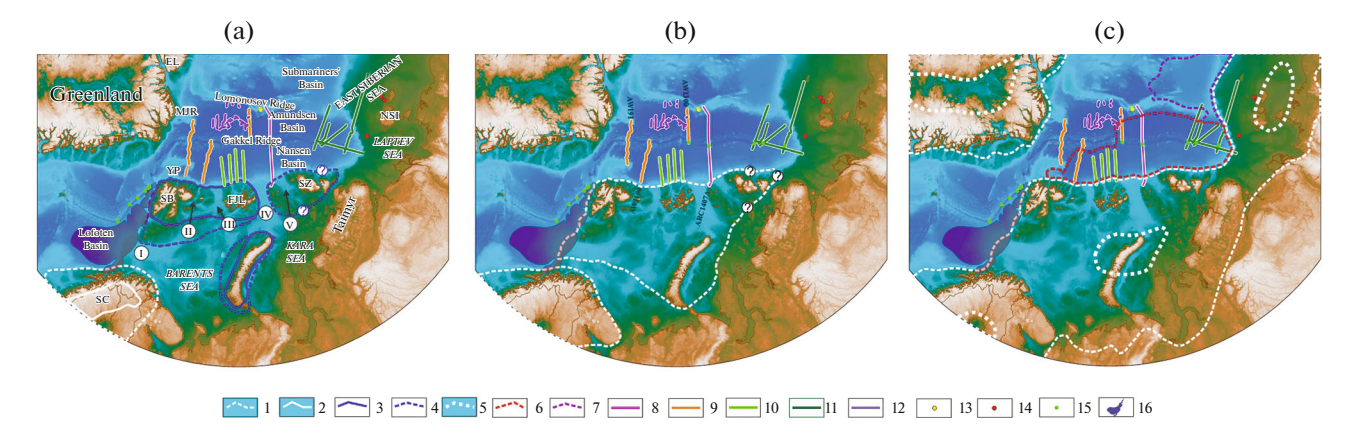


Fig. 8. Model of the main stages of the ice sheet development in the Arctic since Late Pliocenea. Modifies after (Alexandropoulou et al., 2021; Grosswald, 2009; Knies et al., 2009). Based on the IBCAO digital model of relief, v.4 (Jackobson et al., 2020). (a) Stage 1 (~2.7–1.5 Ma BP); (b) stage 2 (~1.5–0.42 Ma BP); (c) stage 3 (<~0.11 Ma BP). Abbreviations: (SC) Scandinavia, (SB) Spitsbergen Archipelago, (FJL) Franz Josef Land Archipelago, (SZ) Severnaya Zemlya Archipelago, (NZ) Novaya Zemlya Archipelago, (NSI) New Siberian Islands, (YP) Yermak Plateau, (MJ) Morris Jesup Rise. (I) Bear Island Trough; (II) Orel Trough; (III) Franz Victoria Trough; (IV) Saint Anna Trough; (V) Voronin Trough. (1-4) Terrains with the maximum and minimum development of ice sheet: (1) maximum (from ~2.7 to ~1.5 Ma BP), (2) minimum (from ~2.7 to ~1.5 Ma BP); (3) maximum (from ~2.7 to ~2.58 Ma BP); (4) maximum (from ~1.95 to ~1.5 Ma BP); (5) ice sheet centers during <~0.11 Ma BP; (6, 7) terrains of glaciomarine deposits with an age of $<\sim 2.7$ Ma in deep-water parts of the Eurasian and Podvodnikov basins: (6) transported from continental margins of the Barents Sea-Kara and Laptev seas, (7) transported from the East Siberian continental margin; (8-12) position of seismic profiles: (8) ARC1407A (Russia), according to (Zayonchek et al., 2023), (9) AWI (Germany), according to (Jokat and Micksch, 2004)), 10) ARC (Russia), according to (Zayonchek et al., 2023), (11) ARC (Russia) sia), according to (Nikishin et al., 2018), (12) Lomrog (Denmark/Canada), according to (Castro et al., 2018); (13, 14) position of boreholes: (13) ACEX, according to (Backman et al., 2006), (14) shallow stratigraphic (Russia), according to (Malyshev et al., 2024); (15) recorded by seismic data on the terrain of glaciomarine deposits in rift valleys of the Knipovich and Mohn ridges, according to (Amundsen et al., 2011; Gusev and Shkarubo, 2001); (16) terrain of glaciomarine deposits in the northeastern Norway-Greenland Basin. The semi-transparent shading outlines Pliocene-Pleistocene landfalls in the northeastern Norway-Greenland Basin, according to (Safronova et al., 2017).

ternary as the main "gateway" for the transport of glaciomarine sediments into the Nansen basin, which is confirmed by the existence of an underwater canyon system on the opposite side extending up to the Gakkel Ridge rift mountains (Fig. 6).

Starting on the eastern flank of the Franz Victoria Trough and the western flank of the Saint Anna Trough, seismic profiles located in the Nansen Basin north of the Franz Josef Land Archipelago (Fig. 8) include large areas marked by the loss of seismic signal correlation, which are interpreted as turbidite flows and landslides (Sokolov et al., 2021; Zayonchek and Merkouriev, 2021). Similar objects are also distinguished on seismic profile AWI 20010100 (Figs. 1, 8) located opposite the Orel Gorge mouth (Engen et al., 2009).

The first glaciomarine sedimentation (~2.7–1.5 Ma) stage, designated GI in (Alexandropoulou et al., 2021; Faleide, 1996), was marked by an avalanche-type accumulation of sediments as underwater landslides (Figs. 2, 8a). We assume that the Kara Glacier, which also occupied the Voronin trough, was formed almost synchronously with the Barents and Novaya Zemlya ice sheets (Fig. 8a). The relief in the Nansen Basin was deeper than at present, apparently, occupied an approximately intermediate position between the modern relief and the lower surface of the assumed

landslide bodies. Comparison of reflections in the middle part of the seismic section reveals differences in incidence angles on both walls of the ridge. In the Amundsen Basin, they fall from the Lomonosov Ridge foothill toward the Gakkel Ridge. On the contrary, they begin to rise on the ridge approximately in the middle of the Nansen Basin. Such geometry indicates subsidence of the Earth's crust because of the impossibility of full compensation due to its own elasticity under the influence of the mass of avalanche-type glaciomarine deposits.

Prior to the glaciomarine stage, sediments delivered to the Nansen basin from the Barents–Kara shelf (Nikishin et al., 2018) should have formed a progradation complex on the continental slope. The alongtrough movement of glaciers toward the Nansen Basin provoked the detachment of older sedimentary sequences on the continental slope and the emergence of underwater landslides. The formation of such structures in the glaciomarine period has been studied well on the Scandinavian continental slope. This segment accommodates about 40 underwater landslide bodies that appeared over the last ~2.7 Ma-4 ka BP (Mazarovich et al., 2024). The world's largest Storegga underwater landslide (Smith et al., 2004) is marked by the wall detachment length of ~290 km. The landslide moved over a distance of about 770 km ~8.2 ka BP.

The observed lower two regions of the loss of seismic signals 1 and 1' correlation (Fig. 7a, Appendix 1), interpreted as submarine landslides, indicate the movement of older sedimentary sequences toward the Gakkel Ridge. Given that impulse 1 of the avalanche-type sedimentation (Fig. 2) is linked with the Norwegian western continental margin of the Barents Sea, it may correspond to stage GI (~2.7–1.5 Ma BP).

Impulse 1 (correlation loss areas 1 and 1', Fig. 7a, Appendix 1) smoothed out the paleorelief in the central Nansen Basin. During impulse 2 (correlation loss areas 2 and 2'), the submarine landslides "lingered" for a while in the lower part of the continental slope, and the relief was smoothed. Upon moving from the basin center toward the Gakkel Ridge, the seismic section shows a transition from the chaotic record to partially chaotic pattern and the subsequent appearance of packages with prominent reflections, suggesting a transition from landfalls to turbidite flows with significant kinetic energy, which allowed them to reach the syn-rift mountains. Bypassing the latter mountains and filling the intermontane depressions, they began to reach the Gakkel Ridge paleorift valley ~1.775 Ma BP. but the maximum intensity was achieved ~0.99 Ma BP (Figs. 7a–7b, Appendix 1). Since the underwater turbidite flows were intense and fast, they almost "flew" over the rift valley and settled on the ridge flank in the Amundsen Basin.

These two impulses, similar in the sedimentation mechanism (submarine landslides), can be considered as cycle 1 (~2.7–0.99 Ma BP) that produced the seismic complex NA-7-I.

The next sedimentation stage (~0.99–0.42 Ma BP) differed significantly from the previous stages. Within the identified seismic complexes (NA-7-II and NA-7-III), only the topmost portion includes the area of partial acoustic turbidity of signal. In general, the time section is characterized by a partial loss of signal coherence. One can see a steady narrowing trend of solitary reflections toward the ridge, possibly indicating the settling of a coarse-grained portion within the continental slope and a higher content of water in flows as they move away from the slope. This cycle was characterized by the predominance of turbidite flows.

The final stage (NA-7-IV, <~0.42 Ma BP) took place under mixed conditions of both turbidite flows and underwater landslides, presumably, due to a change in the ice sheet boundaries and sea level. The existing seismic profile network in the Nansen Basin is not yet sufficient to decipher more detailed fabrics. The ARC14 profiles (Fig. 1) do not extend to the rift valley, and some of them in the northern part are located above seamounts, hampering application of the seismostratigraphic correlation method used in this work.

In our opinion, the seismostratigraphic subdivision of the upper part of the section in the Amundsen Basin remains problematic. The seismic time section (Fig. 7a, Appendix 1) indicates a difference in sedimentation mechanisms in the Amundsen and Nansen basins. According to (Castro et al., 2018), the sediments were delivered to the Amundsen Basin from the northern Greenland shelf in the Late Pleistocene. The geomorphological analysis (Figs. 5, 6) suggests a significant input of sediments into the eastern and central parts of the Amundsen Basin from the Laptev Sea.

Issue of the possible glaciation on the New Siberian Islands and the surrounding East Arctic shelf was debated for many years. One group of scientists proposed the model of Pan-Arctic ice sheet (ice-sheet glaciation of the entire northern Polar region) in the Pleistocene (Grosswald, 2009; Grosswald and Hughes, 1995, 1998; Hughes, 1998; Hughes et al., 1977; Kotlyakov, 1994). Other researchers advocate the concept of "limited glaciation" (Pavlidis et al., 1998; Velichko et al., 1979), admitting the existence of only local ice caps.

Field observations of natural outcrops of Quaternary sediments on the New Siberian Islands, as well as geochemical and isotopic studies of stratified ice caps, confirmed the assumption about the existence of icesheet glaciation (Basilyan and Nikol'sky, 2010), the beginning of which dates back to the second half of the Middle Pleistocene (Golionko et al., 2019), which corresponds to the boundary with an age of ~0.13 Ma (Figs. 2, 7a, 7b).

Shallow stratigraphic drilling accomplished on the northern shelf of Laptev Sea (Figs. 1, 8) was accompanied by ultra-high resolution seismic acoustic survey (Malyshev et al., 2023). Some areas revealed that rocks in the uppermost seismic complex are involved in intense fold-thrust deformations, similar to glaciodynamic deformations on the New Siberian Islands (Verzhbitsky et al., 2024). Although the field of maximum ice sheet in the East Arctic seas is shown in Fig. 8c in accordance with (Grosswald, 2009), its domain remains an open issue. According to (Basilyan and Nikol'sky, 2010), the glaciation centers were represented by the Zhokhov and Bennett Islands of the De Long Archipelago. From these rises, ice could spread in all directions, partially capturing the New Siberian Islands. In this case, the upper part of the sedimentary cover in the Amundsen and Podvodnikov basins can be represented by glaciomarine deposits of the second half of the Middle Pleistocene. In the eastern Nansen Basin near the Laptev Sea coast, where landslide bodies are known on the slope (Kaminsky et al., 2024). probably, glacial sedimentation began earlier in the Late Pliocene.

CONCLUSIONS

1. Significant sedimentary cover thicknesses in the Nansen Basin are composed glaciomarine sediments accumulated since the end of the Late Pliocene.

- 2. Interpretation of the time section of seismic profile ARC1407A allows the possibility of using the seismostratigraphic correlation scheme of glaciomarine deposits developed previously for the western Barents Sea and the northeastern adjacent deepwater basin.
- 3. The geomorphological analysis revealed extended canyon systems in the Nansen Basin and the eastern part of the Amundsen Basin.
- 4. In the central part of the Nansen Basin, glaciomarine sediments were delivered simultaneously from two closely spaced troughs (Saint Anna and Voronin).
- 5. The accumulation of glaciomarine sediments in the central Nansen Basin was characterized by cyclicity, with the submarine landslides and turbidite flows serving as the main suppliers of sedimentary material.
- 6. Glaciomarine deposits of significant thickness are also present in the central and eastern parts of the Gakkel Ridge rift valley.
- 7. In the Amundsen and Podvodnikov basins, the deposition of glaciomarine sediments could begin in the second half of the Middle Pleistocene.

SUPPLEMENTARY INFORMATION

The online version contains supplementary material available at https://doi.org/10.1134/S002449022570021X

ACKNOWLEDGMENTS

The authors are grateful to reviewers N.P. Chamov, DSc (Geol.—Miner.) and I.S. Patina, PhD (Geol.—Miner.) for comments that helped to improve significantly the text and illustrations in the article.

FUNDING

This work was supported by the Russian Science Foundation, project no. 24-17-00097 "The Atlantic—Arctic Rift System: Segmentation, Evolution, Structure Formation, and Modern Geodynamics" (S.Yu. Sokolov, supervisor).

CONFLICT OF INTEREST

The authors of this work declare that they have no conflicts of interest.

REFERENCES

Alexandropoulou, N., Winsborrow, M., Andreassen, K., et al., Continuous seismostratigraphic framework for the western Svalbard—Barents Sea margin over the last 2.7 Ma: Implications for the Late Cenozoic glacial history of the Svalbard—Barents Sea ice sheet, *Front. Earth Sci.*, 2021, vol. 9. 656732.

https://doi.org/10.3389/feart.2021.656732

Amundsen, I.M.H., Blinova, M., Hjelstuen, B.O., et al., The Cenozoic western Svalbard margin: Sediment geometry and sedimentary processes in an area of ultraslow ocean-

ic spreading, *Mar. Geophys. Res.*, 2011, vol. 32, pp. 441–453

Andreassen, K., Nilssen, L.C., Rafaelsen, B., and Kuilman, L., Three-dimensional seismic data from the Barents Sea margin reveal evidence of past ice streams and their dynamics, *Geology*, 2004, vol. 32, pp. 729–732.

Andreassen, K., Odegaard, C. M., and Rafaelsen, B., Imprints of former icem streams, imaged and interpreted using industry three-dimensional seismic data from the southwestern Barents Sea, in *Seismic Geomorphology: Applications to Hydrocarbon Exploration and Production*, Davies, R.J., Posamentier, H.W., Wood, L.J., and Cartwright, J.A., Eds., London: Geol. Soc., 2007, pp. 151–169.

Backman, J., Moran, K., McInroy, D.B., Mayer, L.A., et al., Artic Coring Expedition (ACEX), *Proc. Integr. Ocean Drill. Progr. Leg. 302*, 2006.

https://doi.org/10.2204/iodp.roc.302.2006

Basilyan, A.E., Nikol'skii, P.A., Maksimov, F.E.,and Kuznetsov, V.Yu., Age of traces of sheet glaciation on New Siberian Islands based on ²³⁰Th/U dating of mollusck shells, in *Stroenie i istoriya razvitiya litosfery. Vklad Rossii v Mezhdunarodnyi Polyarnyi God* (Structure and History of the Lithosphere Evolution: Contribution of Russia to the International Polar Year) Leonov, Yu.G., Ed., Moscow: Paulsen, 2010, vol. 4, p. 506–514.

Batchelor, C.L. and Dowdeswell, J.A., The physiography of High Arctic cross-shelf Troughs, *Quat. Sci. Rev.*, 2014, vol. 92, pp. 68–96.

Bonvalot, S., Balmino, G., Briais, A., et al., *World Gravity Map*, BGI-CGMW-CNES-IRD, Comm. Geol. Map World, Paris, 2012. https://bgi.obs-mip.fr/activities/projects/world-gravity-map-wgm.

Bruvoll, V., Breivik, A.J., Mjelde, R., and Pedersen, R.B., Burial of the Mohn-Knipovich seafloor spreading ridge by the Bear Island Fan: Time constraints on tectonic evolution from seismic stratigraphy, *Tectonics*, 2009, vol. 28(4), pp. 1–14.

Butt, F.A., Elverhoi, A., Solheim, A., and Forsberg, C.F., Deciphering late Cenozoic development of the western Svalbard margin from ODP Site 986 results, *Mar. Geol.*, 2000, vol. 169, pp. 373–390.

Castro, C.F., Knutz, P.C., Hopper, J.R., and Funck, T., Depositional evolution of the western Amundsen Basin, Arctic Ocean: Paleoceanographic and tectonic implications *Paleoceanograph. Paleoclimatol.*, 2018, vol. 33. https://doi.org/10.1029/2018PA003414

Channell, J.E.T., Smelror, M., Jansen E., et al., Age models for glacial fan deposits off East Greenland and Svalbard (ODP Site 986 and Site 987), *Proc. ODP Sci. Res.*, 1999, vol. 162, pp. 149–166.

Dessandier, P.-A., Knies, J., Plaza-Faverola, A., Labrousse, C., Renoult, M., Panieri, G., et al., Ice-sheet melt drove methane emissions in the Arctic during the last two interglacials, *Geology*, 2021, vol. 49(7), pp. 799–803.

Eidvin, E. and Nagy, J., Foraminiferal biostratigraphy of Pliocene deposits at Site 986, Svalbard margin, *Proc. ODP Sci. Res.*, 1999, vol. 162, pp. 3–17.

Engen, Ø., Faleide, J.I., and Dyreng, T.K., Opening of the Fram Strait gateway: A review of plate tectonic constraints, *Tectonophysics*, 2008, vol. 450, pp. 51–69.

Engen, Ø., Gjengedal, J.A., Faleide, J.I., et al., Seismic stratigraphy and sediment thickness of the Nansen Basin, Arctic Ocean, *Geophys. J. Int.*, 2009, vol. 176, pp. 805–821. Faleide, J.I., Solheim, A., Fiedler, A., and Vanneste, K., Late Cenozoic evolution of the western Barents Sea–Svalbard continental margin, *Global Planet. Change*, 1996, vol. 12(1–4), pp. 53–74.

Fiedler, A. and Faleide, J.I., Cenozoic sedimentation along the southwestern Barents Sea margin in relation to uplift and erosion of the shelf, *Glob. Planet. Change*, 1996, vol. 12, pp. 75–93.

Forsberg, C.F., Solheim, A., Elverhoi, A., et al., The depositional environment of the western Svalbard margin during the late Pliocene and the Pleistocene: Sedimentary facies changes at Site 986, *Proc. ODP Sci. Res.*, 1999, vol. 162, pp. 233–246.

Gaina, C., Roest, W.R., and Muller, R.D., Late Cretaceous—Cenozoic deformation of northeast Asia, *Earth Planet. Sci. Lett.*, 2002, vol. 197, pp. 273–286.

Geissler, W.H. and Jokat, W., A geophysical study of the northern Svalbard continental margin, *Geophys. J. Int.*, 2004, vol. 158, pp. 50–66.

Glebovsky, V.Yu., Kaminskii, V.D., Minakov, A.N., et al., Formation of the Eurasia Basin in the Arctic Ocean as inferred from geohistorical analysis of the anomalous magnetic field, *Geotectonics*, 2006, no. 4, pp. 263–281.

Golionko, B.G., Basilyan, A.E., Nikol'sky, P.A., et al., Fold—thrust deformations of New Siberia Island (Novosibirsky Islands, Russia): Age, morphology, and genesis of structures, *Geotectonics*, 2019, no. 6, pp. 675–700.

Grosval'd, M.G., Glaciation in the Russian North and Northeast during the Last Great Cooling Epoch, in *Materialy glyatsiologicheskikh issledovanii* (Materials of Glaciological Studies), Kotlyakov, V.M, Ed., Moscow: Nauka, 2009, iss. 106.

Gusev, E.A. and Shkarubo, S.I., Anomalous structure of the Knipovich Ridge, *Ross. Zh. Naul Zemle*, 2001, vol. 3, no. 2, pp. 165–181.

Harishidayat, D., Johansen, S. E., Batchelor, C., et al., Pliocene—Pleistocene glacimarine shelf to slope processes in the south-western Barents Sea, *Basin Res*, 2005, vol. 22(2), pp. 1315—1336.

Hjelstuen, B.O., Eldholm, O., and Faleide, J.I., Recurrent Pleistocene megafailures on the SW Barents Sea margin, *Earth Planet. Sci. Lett.*, 2007, vol. 258, pp. 605–618.

Jakobsson, M., Mayer, L.A., Bringensparr, C., et al., *The International Bathymetric Chart of the Arctic Ocean. Version 4.0 Scientific Data*, 2020, vol. 176(7).

https://doi.org/10.1038/s41597-020-0520-9

Jokat, W. and Micksch, U., Sedimentary structure of the Nansen and Amundsen basins, *Arctic Ocean Geophys. Res. Lett.*, 2004, vol. 31(2), pp. 1–4.

Jansen, E., Raymo, M. E., and Blum, P., The Leg 162 Shipboard Scientific Party, *Proc. Ocean Drill. Progr.*, 1996, vol. 162.

Kaminsky, D.V., Chamov, N.P., Zhilin, D.M., et al., New data on the structure of the Laptev Sea flank of the Gakkel Ridge (Arctic Ocean), *Lithol. Miner. Resourc.*, 2024, vol. 59, no. 6, pp. 598–610.

Karasik, A.M., The Eurasian Basin in the Arctic Ocean form the perspective of the Plate tectonics, in *Problemy geologii polyarnykh oblastei Zemli* (Problems in the Geology

of Polar Regions in the Earth), Gramberg, I.S, Lazurkin, V.M, Ravich, M.G, and Tkachenko, B.V, Eds., Leningrad: NIIGA, 1974, pp. 23–31.

Kitamura, A. and Kawagoe, T., Eustatic sea-level change at the Mid-Pleistocene climate transition: new evidence from the shallow-marine sediment record of Japan, *Quat. Sci. Rev.*, 2006, vol. 25, pp. 323–335.

Knies, J., Matthiessen, J., Vogt, C., Laberg, J.S., et al., The Plio-Pleistocene glaciation of the Barents Sea—Svalbard region: a new model based on revised chronostratigraphy, *Quat. Sci. Rev.*, 2009, vol. 28(9), pp. 812–829.

Laberg, J.S., Andreassen, K., Knies, J., Vorren, T.O., and Winsborrow, M., Late Pliocene—Pleistocene development of the Barents Sea ice sheet, *Geology*, 2010, vol. 38, pp. 107—110.

Lasabuda, A.P.E., Johansen, N.S., and Laberg, J.S., Cenozoic uplift and erosion of the Norwegian Barents Shelf—A review, *Earth-Sci. Rev.*, 2021, vol. 217. 103609. http://doi.https://doi.org/10.1016/j.earscirev.2021.103609

Malyshev, N.A., Verzhbitsky, V.E., Danilkin, S.M., et al., Stratigraphic drilling in the northeastern part of Laptev Sea, *Dokl. Earth Sci.*, 2024, vol. 515, no. 1, pp. 563–572. https://doi.org/10.31857/S2686739724030048

Mattingsdal, R., Knies, J., Andreassen, K., Fabian, K., Husum, K., Grosfjeld, K., et al., A new 6 Myr stratigraphic framework for the Atlantic-Arctic Gateway, *Quat. Sci. Rev.*, 2014, vol. 92, pp. 170–178.

Mazarovich, A.O., Abramova, A.S., Dobrolyubova, K.O., et al., Probability of the formation of landfalls at the Norway continental margin, *Vestn. KRAUNTs. Nauki Zemle*, 2024, iss. 61, no. 1, pp. 42–56.

Medvedev, S., Faleide, J.I., and Hartz, E.H., Cenozoic reshaping of the Barents-Kara Shelf: Influence of erosion, sedimentation, and glaciation, *Geomorphology*, 2023, vol. 420.

https://doi.org/10.1016/j.geomorph.2022.108500

Merkouriev, S. and DeMets, C., High-resolution Quaternary and Neogene reconstructions of Eurasia–North America plate motion, *Geophys. J. Int.*, 2014, vol. 198, pp. 366–384.

Michael, P.J., Langmuir, C.H., Dick, H.J.B., et al., Magmatic and amagmatic seafloor generation at the ultraslow-spreading Gakkel ridge, Arctic Ocean, *Nature*, 2003, vol. 423(6943), pp. 956–961.

Moore, I.D. and Neiber, J.L., Landscape assessment of soil erosion and non-point source pollution, *J. Minn. Acad. Sci.*, 1989, vol. 55, pp. 18–24.

Mudelsee, M. and Stattegger, K., Exploring the structure of the mid-Pleistocene revolution with advanced methods of time-series analysis, *Geol. Rundsch.*, 1997, vol. 86, pp. 499–511

Myhre, A., Thiede, J., and Firth, J.A., North Atlantic Arctic Gateways, *Proc. ODP Init. Rep.*, 1995, vol. 151, pp. 1–81. Nikishin, A.M., Gaina, C., Petrov, E.I., et al., Eurasia Basin and Gakkel Ridge, Arctic Ocean: Crustal asymmetry, ultra-slow spreading and continental rifting revealed by new seismic data, *Tectonophysics*, 2018, vol. 746, pp. 64–82.

Pontbriand, C.W., Soule, S.A., Sohn, R.A., Humphris, S.E., Kunz, C., Singh, H., Nakamura, K., Jakobsson, M., and Shank, T., Effusive and explosive volcanism on the ultraslow-spreading Gakkel Ridge, 85° E, *Geochem. Geophys.*

Geosyst., 2012, vol. 13(10), pp. 1–22. https://doi.org/10.1029/2012GC004187

Rebesco, M., Laberg, J.S., Pedrosa M.T., et al., Onset and growth of Trough-Mouth Fans on the North-Western Barents Sea margin—implications for the evolution of the Barents Sea/Svalbard ice sheet, *Quat. Sci. Rev.*, 2014, vol. 92, pp. 227–234.

Rekant, P.V. and Gusev, E.A., Structure and History of the formation of sedimentary cover in the rift zone of the Gakkel Ridge (Northern Arctic Ocean), *Geol. Geofiz.*, 2016, vol. 57, no. 9, pp. 1634–1640.

Rekant, P.V., Petrov, O.V., and Gusev, E.A., Model of formation of the sedimentary system of the Eurasian Basin, the Arctic Ocean, as a basis for reconstructing its tectonic evolution, *Geotectonics*, 2021, no. 5, pp. 676–696.

Safronova, P.A., Laberg, J.S., Andreassen, K., et al., Late Pliocene-early Pleistocene deep-sea basin sedimentation at high-latitudes: mega-scale submarine slides of the north-western Barents Sea margin prior to the shelf-edge glaciations, *Basin Res.*, 2017, vol. 29, pp. 537–555.

Smith, D.E., Shi, S., Cullingford, R.A., et al., The Holocene Storegga Slide tsunami in the United Kingdom, *Quat. Sci. Rev.*, 2004, vol. 23(23–24), pp. 2291–2321. https://doi.org/10.1016/j.quascirev.2004.04.001

Sokolov, S.Yu., Moroz, E.A., Chamov, N.P., and Patina, I.S., Paleogen—Quaternary polyfacies sedimentary system of the southern Nansen Basin, *Lithol. Miner. Resourc.*, 2021, no. 5, pp. 375—389.

The Geologic Time Scale, Gradstein, F.M., Ogg, J.C., Smith, M.D., and Ogg, G.M., Eds., Oxford: Elsevier, 2020. Velichko, A.A., Problems in the reconstruction of Late Neopleistocene glacial sheets in the Soviet Union, *Izv. AN SSSR. Ser. Geogr.*, 1979, no. 6, pp. 12–26.

Verzhbitsky, V.E., Malyshev, N.A., Kolyubakin, A.A., et al., New data on the tectonics of the northeastern Laptev Sea (based on the results of expedition studies and stratigraphic drilling), in *Tektonika i geodinamika Zemnoi kory i mantii: fundamental'nye problemy-2024* (Tectonics and Geodynamics of the Earth's Crust and Mantle: Fundamental Problems—2024), Degtyarev, K.E., Ed., Moscow: GEOS, 2924, vol. 1, pp. 80—86.

Vorren, T.O. and Laberg, J.S., Trough mouth fans – palae-oclimate and ice-sheet monitors, *Quat. Sci. Rev.*, 1997, vol. 16, pp. 865–881.

Waage, M., Bünz, S., Bøe, R., and Mienert, J., High-resolution 3D seismic exhibits new insights into the middle-late Pleistocene stratigraphic evolution and sedimentary processes of the Bear Island trough mouth fan, *Mar. Geol.*, 2018, vol. 403 P. 139–149.

Zayonchek, A.V. and Merkouriev, S.A., New results of the identification of linear magnetic anomalies in the western Nansen Basin and its stratigraphic implication for the seismostratigraphic analysis, in *Geologiya morei i okeanov* (Geology of Seas and Oceans), Moscow: IO RAN, 2021, vol. 4, pp. 70–74.

Zayonchek, A.V., Sokolov, S.Yu., and Solov'ev, A.V., The pre-Quaternary evolution of the Eaurasia Basin: The results of interpretation od seismic profile ARC1407A, *Geotectonics*, 2023, no. 6, pp. 693–725.

Translated by D. Sakya

Publisher's Note. Pleiades Publishing remains neutral with regard to jurisdictional claims in published maps and institutional affiliations.

AI tools may have been used in the translation or editing of this article.